# Electronic and optical properties of $\Theta$-$Al_2O_3$ and comparison to $\alpha$-$Al_2O_3$

Shang-Di Mo
*Department of Physics, University of Missouri-Kansas City, Kansas City, Missouri 64110*

W. Y. Ching
*Department of Physics, University of Missouri-Kansas City, Kansas City, Missouri 64110*
*and Max-Plank Institute für Metallforschung, Seestrasse 92, D-70714 Stuttgart, Germany*
(Received 15 December 1997)

$\Theta$-$Al_2O_3$ is a metastable phase of alumina with local Al coordinations closely related to those in $\gamma$-$Al_2O_3$. The electronic structure and the linear optical properties of $\Theta$-$Al_2O_3$ are studied by means of first-principles local density calculations. The results are compared with the stable phase $\alpha$-$Al_2O_3$. An indirect band gap of 4.64 eV is obtained, which is about 1.6 eV smaller than that of $\alpha$-$Al_2O_3$. The other band structure parameters are found to be quite close, and the calculated density of states (DOS) differ from that of $\alpha$-$Al_2O_3$ in fine details. Site- and orbital-resolved partial DOS show significant dependence on local coordinations for both Al and O atoms. They are in reasonable agreement with the experimental energy loss near edge spectra of $\gamma$-$Al_2O_3$. Effective charge and bond order calculations show $\Theta$-$Al_2O_3$ to be comparable to $\alpha$-$Al_2O_3$. For the linear optical properties, a refractive index 1.73 is obtained, which is close to 1.78 for $\alpha$-$Al_2O_3$. The bulk plasmon peak in the energy loss function of $\Theta$-$Al_2O_3$ is located at 22.6 eV, which is lower by about 1 eV than that in $\alpha$-$Al_2O_3$. The anisotropy in the optical properties of $\alpha$-$Al_2O_3$ occurs mainly at the low photon energy region of less than 20 eV, and that for the $\Theta$-$Al_2O_3$ is insignificant. [S0163-1829(98)00424-X]

## I. INTRODUCTION

Alumina ($Al_2O_3$) or sapphire is one of the most important ceramic materials with exceptional properties[1–3] such as great hardness, chemical inertness, and a high melting temperature. It has many industrial applications such as in catalysis, coatings, microelectronics, composite materials, and advanced material technology. Besides the stable phase $\alpha$-$Al_2O_3$, alumina can also exist in a number of metastable polymorphs.[4] The structures of the metastable aluminas, also called transition aluminas, can be divided into two distinct categories based on either a fcc or a hcp arrangement of the anions. Among them, $\alpha$-$Al_2O_3$ has a hcp structure, while $\gamma$-$Al_2O_3$ belongs to the fcc structure. Due to its technological importance, $\alpha$-$Al_2O_3$ has been well studied both theoretically and experimentally in recent years.[3,5–10] These studies include the confirmation of microstructures and determination of various properties. Recently, Tanaka and Adachi[5] have calculated the Al $L_{2,3}$-edge x-ray-absorption spectra of $\alpha$-$Al_2O_3$ by a cluster molecular-orbital method with a core-hole excitonic feature included. Boettger[6] presented a high-precision all electron full-potential calculation of the equation of state and elastic constants for $\alpha$-$Al_2O_3$. The calculated lattice parameters and zero-pressure elastic properties are in extraordinary agreement with the existing experiment data. In large scale molecular dynamics simulations,[7] Thomson *et al.* showed that phase transformations in $Al_2O_3$ at high pressure are possible, and other polymorphs of alumina were predicted. Very recently, a plane-wave pseudopotential calculation[8] was carried out to investigate the possible structures of $\kappa$-$Al_2O_3$ by Yourdshahyan *et al.* They concluded that structures with sixfold coordinated Al are significantly more stable than that with fourfold coordinated Al. Experimental measurement on optical spectra of $\alpha$-$Al_2O_3$ single crystal has been carried out by Tomiki *et al.*[9] The anisotropic optical properties have been discussed in considerable detail. The optical properties of $\alpha$-$Al_2O_3$ have also been investigated by French *et al.*[10] over the energy range of 6 to 142 eV, using two independent methods, vacuum ultraviolet (VUV) and electron energy loss spectroscopy (EELS).

A few years ago, Ching and Xu[11] presented a theoretical study of the electronic, structural, and optical properties of $\alpha$-$Al_2O_3$ in corundum structure by means of first-principles local density calculations. An indirect energy band gap of 6.29 eV was obtained. The calculated density of states (DOS) were compared with x-ray photoemission and photoabsorption measurements. The highly ionic feature of $\alpha$-$Al_2O_3$ was shown by real space charge density analysis. The calculated ground-state properties showed excellent agreement with experimental data. The calculated optical absorption spectrum was also in general agreement with the experimental VUV data.

In contrast to $\alpha$-$Al_2O_3$, there has been much less study on $\gamma$-$Al_2O_3$, although it has important applications in catalysis.[12] Up to now, the basic structural properties of $\gamma$-$Al_2O_3$ is still not very clear. The prevailing understanding is that $\gamma$-$Al_2O_3$ is a defective spinel with vacancies on cation sites and two types of cation coordinations, the octahedral coordination Al-$O_6$ and the tetrahedral coordination Al-$O_4$. In $\alpha$-$Al_2O_3$ there is only Al-$O_6$ coordination. There exists a long-standing controversy as to whether the vacancies should occupy the octahedral or the tetrahedral sites. In our recent work,[13] we used an empirical pair potential to model the structure of $\gamma$-$Al_2O_3$, followed by DOS calculation.[13] It was tentatively concluded that the cation vacancy prefers the oc-

 

TABLE I. Crystal structures of $\alpha$- and $\Theta$-$Al_2O_3$.

| | $\alpha$-$Al_2O_3$ (Ref. 19) | $\Theta$-$Al_2O_3$ (Ref. 15) | $\Theta$-$Al_2O_3$ (Ref. 16) |
|---|---|---|---|
| Crystal structure | Rhombohedral | Monoclinic | Monoclinic |
| Molecules/cell | 2 | 4 | 4 |
| Lattice constant (Å) | $a=5.128$ | $a=11.854$ | $a=11.795$ |
| | $\alpha=55.333°$ | $b=2.904$ | $b=2.910$ |
| | | $c=5.622$ | $c=5.621$ |
| | | $\beta=103.83°$ | $\beta=103.79°$ |
| Space group | $R3C$ | $C2/m$ | $C2/m$ |
| Density (gm/cm$^3$) | 3.984 | 3.3604 | 3.615 |
| Unit cell volume (Å$^3$) | 85.013 | 187.921 | 187.371 |
| | | $t$: 1.710 (2) | $t$: 1.70 (1) |
| | | 1.745 (1) | 1.79 (2) |
| | | 1.811 (1) | 1.81 (1) |
| Al-O bonds (Å)[a] | | | |
| | $o$: 1.857 (3) | $o$: 1.897 (1) | $o$: 1.82 (1) |
| | 1.969 (3) | 1.904 (2) | 1.84 (2) |
| | | 1.936 (1) | 1.99 (2) |
| | | 2.025 (2) | 2.09 (1) |

[a] $t(o)$ represents tetrahedral (octahedral) bonds. The numbers in parentheses are the multiplicity of the Al-O bond.

tahedral site. With a defective spinel structure, $\gamma$-$Al_2O_3$ is much more complicated than $\alpha$-$Al_2O_3$. With the cation vacancies further involved, investigation on the properties of $\gamma$-$Al_2O_3$ becomes a much more formidable task. On the other hand, it is known that $\Theta$-$Al_2O_3$, a metastable precursor phase of $\alpha$-$Al_2O_3$ has a similar local coordination to $\gamma$-$Al_2O_3$.[4] It is also known that a common transformation sequence from $\gamma$-$Al_2O_3$ to $\alpha$-$Al_2O_3$ involves the $\Theta$-$Al_2O_3$ phase.[14] Similar to $\alpha$-$Al_2O_3$, $\Theta$-$Al_2O_3$ is an ordered phase, so its electronic and optical properties can be calculated unambiguously. A good understanding of the electronic and optical properties of $\Theta$-$Al_2O_3$ would certainly aid to the elucidation of $\gamma$-$Al_2O_3$ in general.

The crystal structures and the transformation mechanisms among the $\eta$, $\gamma$, and $\Theta$ phases have been studied by x-ray and neutron powder diffraction by Zhou and Snyder.[15] The profile analysis of various reflection zones in the defective spinel structure shows different coherent domain sizes, which can be associated with the tetrahedral and octahedral Al sites within the O sublattice. The authors are of the opinion that the transition aluminas should be considered spinel deformed rather than tetragonal deformed. The crystal structure of $\Theta$-$Al_2O_3$ has also been investigated by SEM, x-ray and electron diffraction, HRTEM, and vibrational spectroscopy by Husson and Replin.[16] A similar set of crystal parameters as that of Ref. 15 was obtained and the structural similarities among the $\delta$, $\Theta$, and $\gamma$ phases were discussed. On the theory side, the structure and bonding in $\Theta$-$Al_2O_3$ has been investigated at the *ab initio* level by Borosy and co-workers using the periodic Hartree-Fock (HF) method.[17] The optimized structure of $\Theta$-$Al_2O_3$ in the HF calculation was found to be in very good agreement with the crystallographic data. In a recent work, Wilson *et al.*[18] developed a transferable interatomic potential model for simulations in $Al_2O_3$. They used a shell model, a compressible ion model, as well as a compressible ion model with both dipole and quardrupolar polarizability of the $O^{-2}$ ions to calculate the energy difference between $\alpha$- and $\Theta$-$Al_2O_3$. The $\Theta$-$Al_2O_3$ phase was found to be less stable. They also concluded that the compressible O ion is the origin for stabilizing the $\alpha$ structure with respect to the $\Theta$ structure.

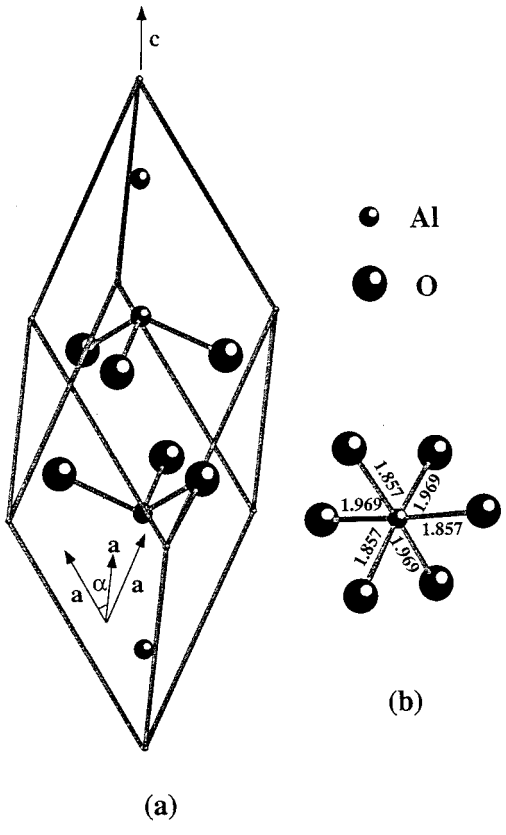


FIG. 1. (a) Rhombohedral unit cell of $\alpha$-$Al_2O_3$; (b) Al-$O_6$ coordination. Al-O bond lengths in Å.

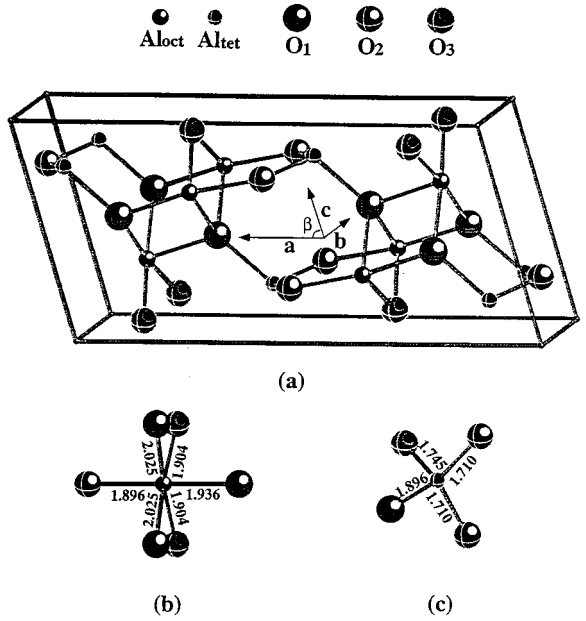


FIG. 2. (a) Monoclinic unit cell of Θ-$Al_2O_3$; (b) Al-$O_6$ coordination; (c) Al-$O_4$ coordination. Al-O bond lengths in Å. $O_1$, $O_2$, $O_3$ are the O atoms with different local coordinations (see text).

In the present paper, we report the electronic and optical properties of crystalline Θ-$Al_2O_3$, and then compare the results with the corresponding properties of $\alpha$-$Al_2O_3$. The paper is organized as follows. In Sec. II, we describe the crystal structures of Θ- and $\alpha$-$Al_2O_3$ and analyze their local coordinations. In Sec. III, we briefly outline our method of calculation. The calculated results which include the band structures, total energies, DOS and partial DOS (PDOS), effective charges, bond orders, and optical properties are presented in Sec. IV. A summary and some conclusions are given in the last section.

## II. CRYSTAL STRUCTURES

The crystal structures of $\alpha$- and Θ-$Al_2O_3$ used in the present calculation and their interionic distances are summarized in Table I. For $\alpha$-$Al_2O_3$, we used the data given by Wyckoff.[19] $\alpha$-$Al_2O_3$ has a corundum structure with a rhombohedral unit cell containing two $Al_2O_3$ molecules. Its unit cell and cation coordination are shown in Figs. 1(a) and 1(b), respectively. The coordinations are such that an Al atom is surrounded by six O atoms of two different nearest-neighbor (NN) distances, and each O atom has four NN Al atoms. The corundum structure can also be visualized in a hexagonal lattice having six layers of close-packed O atoms with the smaller Al atoms located inside the octahedrally coordinated holes.[20] In this picture, the unit cell in the hexagonal lattice will be three times as large as the rhombohedral cell.

The crystal structure of Θ-$Al_2O_3$ is monoclinic with a space group of $C2/m$. The unit cell contains four $Al_2O_3$ molecules. The crystal parameters have been determined recently by two groups.[15,16] As shown in Table I, the two measurements give very similar lattice parameters $a$, $b$, $c$, and $\beta$ for Θ-$Al_2O_3$. However, the internal parameters and hence the Al-O bond lengths show some differences. It is noted that the density of Θ-$Al_2O_3$ is 10% lower than that of $\alpha$-$Al_2O_3$. The present calculation is based on the lattice parameters of Ref. 15. The monoclinic unit cell of Θ-$Al_2O_3$ is shown in Fig. 2(a). Figures 2(b) and 2(c) show the two types of cation coordination in Θ-$Al_2O_3$. The Al-O bond lengths are given in Table I. They are between 1.710 and 1.811 Å in Al-$O_4$ and between 1.897 and 2.025 Å in Al-$O_6$. In contrast to only one type of O coordination in $\alpha$-$Al_2O_3$, Θ-$Al_2O_3$ has three types of O coordinations. $O_1$ is bonded to one $Al_{tet}$ and three $Al_{oct}$ cations, where $Al_{oct}(Al_{tet})$ stands for the Al in octahedral (tetrahedral) coordination. $O_2$ is bonded to two $Al_{tet}$ and one $Al_{oct}$ cations. $O_3$ is bonded to one $Al_{tet}$ and two $Al_{oct}$ cations. The difference in the local coordinations between $\alpha$- and Θ-$Al_2O_3$ is the origin of the differences in the structures and properties.

## III. METHOD OF CALCULATION

The electronic structure and optical properties of Θ- and $\alpha$-$Al_2O_3$ were calculated using the first-principles self-consistent orthogonalized linear combination of atomic orbitals (OLCAO) method in the local density approximation (LDA). Since the OLCAO-LDA method has been well described elsewhere,[21] we only briefly outline the procedures relevant to the present calculation. The same method has been successfully applied to the study of electronic and optical properties of many inorganic crystals.[22–27]

The basis functions for the band structure calculation are the Bloch sums which were constructed from the atomiclike orbitals of Al ($1s$, $2s$, $2p$, $3s$, $3p$, $4s$, $4p$, and $3d$, with $1s$, $2s$, and $2p$ treated as core), and O ($1s$, $2s$, $2p$, $3s$, $3p$, with $1s$ treated as core). The core states were eliminated by the orthogonalization to the core process to facilitate the calculation. These functions were chosen to be the same as in the previous calculation for $\alpha$-$Al_2O_3$ (Ref. 11), and is referred to as a full-basis calculation. All atomic orbitals were expressed as a linear combinations of Gaussian-type orbitals (GTO's) with a fixed set of exponentials. The valence and the unoccupied orbital Bloch sums were orthogonalized to all the core Bloch sums of all the atoms in the unit cell. The potential and the charge density of the crystal were represented by the superposition of atom-centered functions consisting of simple Gaussians. After the self-consistency in potential was achieved, the band secular equations were solved at 308 and 216 $k$ points in the irreducible portion of the Brillouin zone (BZ) for $\alpha$- and Θ-$Al_2O_3$, respectively. The energy eigenvalues and wave functions were used for the DOS and optical properties calculations. The total energy was evaluated according to the LDA expression

$$E=\sum_{n,k}^{\text{occ}} E_n(k)+\int \rho(r)(\varepsilon_{\text{xc}}-V_{\text{xc}}-V_{ee}/2)dr$$

$$+\sum_{\alpha,\beta} Z_\alpha Z_\beta/(R_\alpha-R_\beta), \tag{1}$$

where $E_n$ is the $n$th band energy, $\rho(r)$ is the electron charge density, and $\varepsilon_{\text{xc}}$ is the exchange-correlation energy functional. $V_{\text{xc}}$ and $V_{ee}$ are the exchange-correlation and Coulomb potentials. $Z_\alpha$ is the nuclear charge of the atom at the lattice point $R_\alpha$. The DOS's were calculated by using the linear analytical tetrahedron method.[28] The PDOS's were ob-

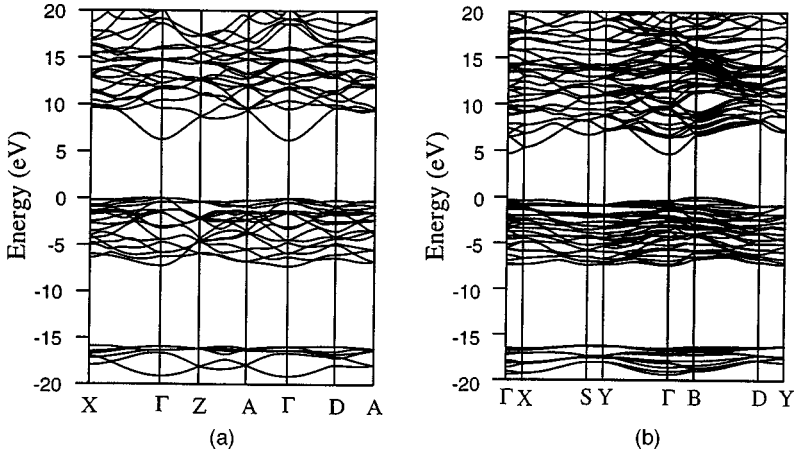


FIG. 3. Calculated band structure of (a) $\alpha$-$Al_2O_3$; (b) $\Theta$-$Al_2O_3$.

tained using the Mulliken scheme.[29] For optical properties, we first calculated the interband optical conductivity $\sigma$ according to the expression

$$\sigma(E)=\frac{e^2}{(2\pi)^2 mE}\int dk\sum |\langle\psi_n(k,r)\rangle|\mathbf{P}|\langle\psi_l(k,r)\rangle|^2 f_l(k) \times[1-f_n(k)]\delta[E_n(k)-E_l(k)-E], \quad (2)$$

where $f_n$ is the Fermi function for state $n$. The momentum matrix elements $|\langle\psi_n(k,r)\rangle|\mathbf{P}|\langle\psi_l(k,r)\rangle|$ at each $k$ point between the Bloch functions were evaluated explicitly. The imaginary part of the dielectric function $\varepsilon_2$ is related to $\sigma(\omega)$ through $\varepsilon_2(\omega)=4\pi\sigma(\omega)/\omega$, and the real part of the dielectric function can be obtained through the Kramers-Kronig relation. The energy loss function $-\mathrm{Im}(1/\varepsilon)$, the index of refraction, and the refractivity spectrum can all be obtained from the complex dielectric function.

## IV. RESULTS

### A. Band structures and total energy

The calculated band structures for $\alpha$- and $\Theta$-$Al_2O_3$ along the high-symmetry lines of the BZ are shown in Figs. 3(a) and 3(b), respectively. For $\alpha$-$Al_2O_3$, the calculated band gap of 6.24 eV is indirect. The bottom of the conduction band (CB) is at $\Gamma$ and the top of the valence band (VB) is at a point along $\Gamma\rightarrow X$ close to $\Gamma$. The direct gap at $\Gamma$ is 6.26 eV. The difference between the direct and indirect band gaps is so small that for all practical purposes, $\alpha$-$Al_2O_3$ is considered as a direct band gap insulator. The often quoted experimental gap for $\alpha$-$Al_2O_3$ is 8.7 eV from optical measurement.[30] This discrepancy is generally attributed to the inadequacy of the LDA theory which is more valid for the ground state properties. In fact, the precise value of the gap in $\alpha$-$Al_2O_3$ is still not known because of the existence of an excitonic peak near the absorption edge.[30] The upper VB width for $\alpha$-$Al_2O_3$ is 7.27 eV and the lower O-2$s$ band width is 3.24 eV. All the above results are almost identical to the earlier calculation.[11]

For $\Theta$-$Al_2O_3$, we obtained a direct band gap of 4.98 eV at $\Gamma$, which is about 1.3 eV smaller than in of $\alpha$-$Al_2O_3$. The minimal band gap of 4.64 eV is between the bottom of the CB at $\Gamma$ and the top of VB at $B$. As with $\alpha$-$Al_2O_3$, the top of the VB is very flat, indicating a very large effective hole mass. The upper VB, consisting mostly of the O-2$p$ orbitals, is 7.41 eV wide and is separated from the low O-2$s$ band of

TABLE II. Calculated band structures of $\alpha$- and $\Theta$-$Al_2O_3$.

| | $\alpha$-$Al_2O_3$ | $\Theta$-$Al_2O_3$ |
|---|---|---|
| Band gap (eV) | 6.24 (indirect) | 4.64 (indirect) |
| | 6.26 (direct) | 4.98 (direct) |
| Top of VB | close to $\Gamma$ | $\Gamma$ |
| Bottom of CB | $\Gamma$ | B |
| Upper VB width (eV) | 7.27 | 7.41 |
| O-2$s$ bandwidth (eV) | 3.24 | 3.14 |
| Gap between upper VB and O-2$s$ band (eV) | 8.63 | 8.86 |

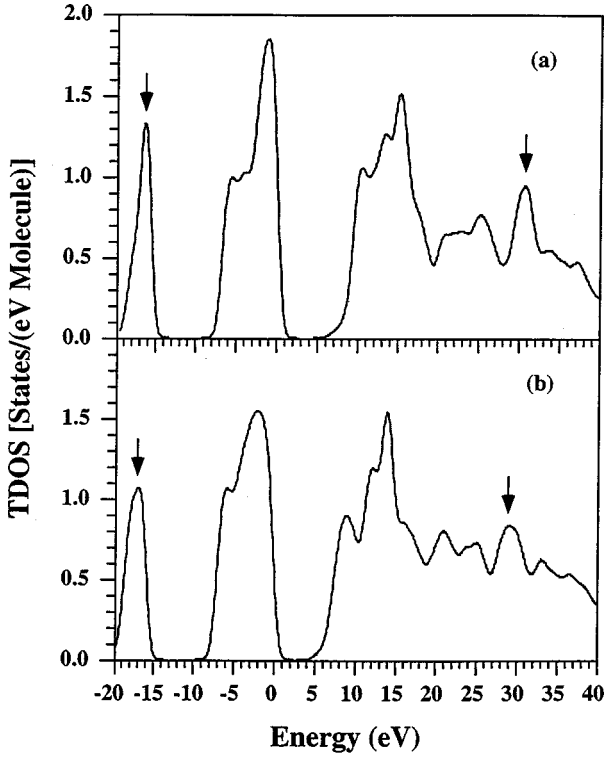


FIG. 4. Calculated total DOS of (a) $\alpha$-$Al_2O_3$; (b) $\Theta$-$Al_2O_3$.

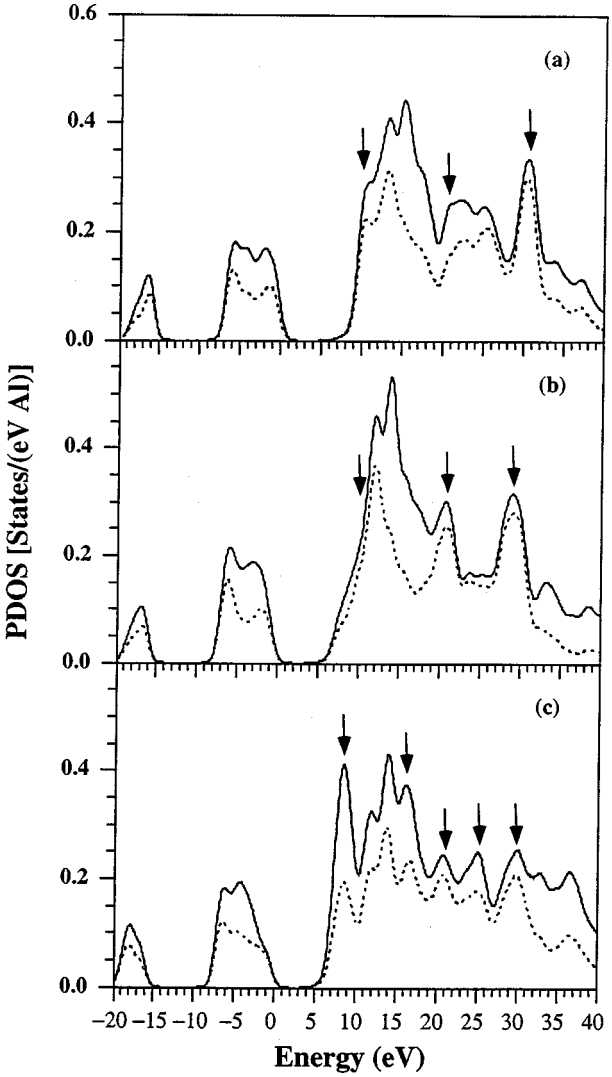


FIG. 5. Calculated PDOS of (a) $Al_{oct}$ in $\alpha$-$Al_2O_3$; (b) $Al_{oct}$ in $\Theta$-$Al_2O_3$; (c) $Al_{tet}$ in $\Theta$-$Al_2O_3$. Dotted lines stand for the sum of *s* and *d* components.

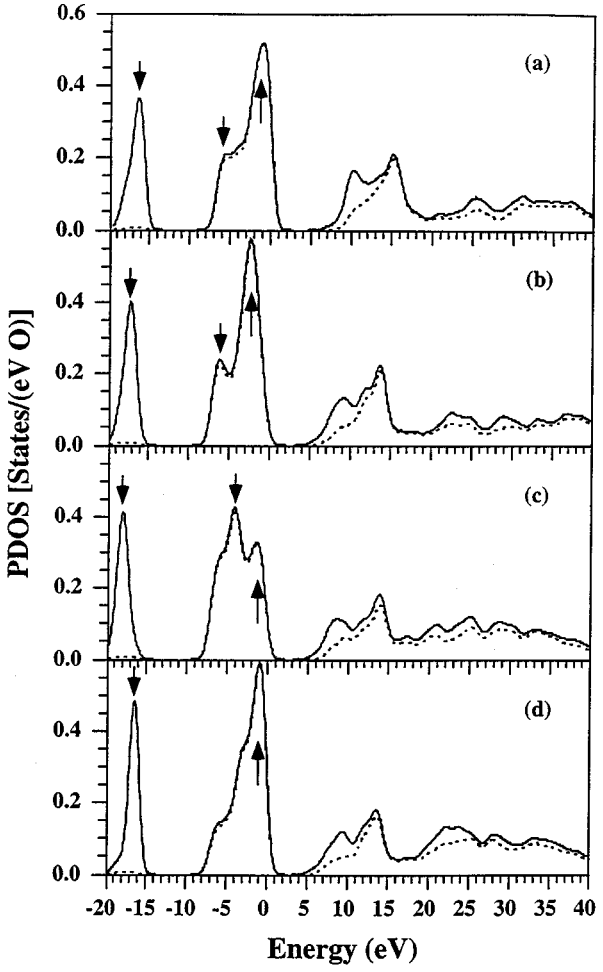


FIG. 6. Calculated PDOS of (a) O in $\alpha$-$Al_2O_3$ and $O_1$ (b), $O_2$ (c), and $O_3$ (d) in $\Theta$-$Al_2O_3$. Dotted lines represent the O-*p* component.

3.14 eV width by a large gap of 8.86 eV. As listed in Table II, except for the fact that $\alpha$-$Al_2O_3$ has a larger direct band gap, the other band parameters for $\alpha$- and $\Theta$-$Al_2O_3$ are very close. A band structure calculation on $\Theta$-$Al_2O_3$ using periodic HF method was presented in Ref. 17. Their result is somewhat different from ours. It is not clear to us why Ref. 17 used a unit cell containing only ten atoms. The monoclinic cell with a space group of $C2/m$ apparently has no inversion symmetry, and should contain four molecules in the unit cell. In contrast to the HF calculation, we find the inclusion of Al-3*d* orbitals to be extremely important in the proper description of bonding in this crystal.

Our total energy calculation shows $\alpha$-$Al_2O_3$ has a lower energy than $\Theta$-$Al_2O_3$ by 1.47 eV per molecule. This translates into an energy difference of 142 kJ $mol^{-1}$ between the $\Theta$ and $\alpha$ phases. (Here, $mol^{-1}$ is interpreted in the sense of per formula unit.) Wilson *et al.*[18] have investigated the energy differences between $\Theta$ and $\alpha$ phases by using a variety of potential models. Their calculated difference ranges from 27.7 to 156 kJ $mol^{-1}$. Their LDA based calculations show a smaller range, from 55.0 to 76 kJ $mol^{-1}$. The HF calculation[17] gives an energy difference of 42 kJ $mol^{-1}$ between $\Theta$ and $\alpha$ phases. All the above calculations using different methods show the $\Theta$ phase to have a higher energy than the $\alpha$ phase. It must be pointed out that some of the difference in the total energy may be attributed to the different crystal parameters used in the calculation for $\Theta$-$Al_2O_3$. Also, in the present calculation for the total energy, the experimental crystal structure was used. We expect the difference in total energy per molecule between $\alpha$-$Al_2O_3$ and $\Theta$-$Al_2O_3$ to be smaller if both structures were optimized within the LDA formalism.

### B. DOS, PDOS, and comparison with ELNES

Figure 4 compares the calculated total DOS of $\alpha$-$Al_2O_3$ and $\Theta$-$Al_2O_3$. The curves have been broadened by a Lorentzian factor of 0.8 to facilitate comparison. The general features of the two DOS curves are similar since they all reflect Al-O bonding. The lower valence band (LVB) is composed of the O-2*s* orbitals, and the upper valence band (UVB) consists mostly of the O-2*p* orbitals, with small mixing from Al-3*s*, -3*p*, and -3*d* hybridized orbitals. The upper part of the UVB corresponds to the O-2*p* nonbonding states, and the lower part is from the O-2*p* bonding states. Al states

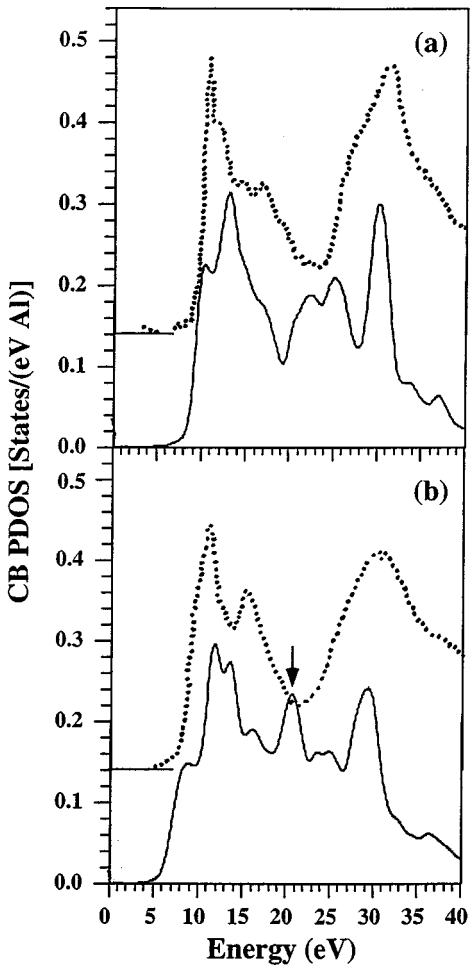


FIG. 7. Comparison of the calculated Al $(s+d)$ PDOS (solid lines) and the experimental (Ref. 32) Al $L_{2,3}$ spectra (dotted lines) in (a) $\alpha$-$Al_2O_3$; (b) $\Theta$-$Al_2O_3$. The Al $L_{2,3}$ of $\gamma$-$Al_2O_3$ is used as an approximation to $\Theta$-$Al_2O_3$.

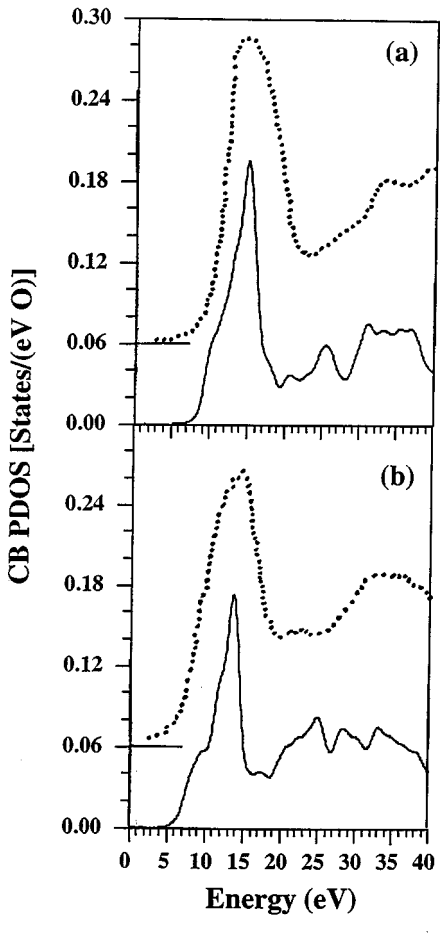


FIG. 8. Comparison of the calculated O-$p$ PDOS (solid lines) of O and the experimental (Ref. 32) O $K$ edge spectra (dotted lines) in (a) $\alpha$-$Al_2O_3$; (b) $\Theta$-$Al_2O_3$. The O $K$ spectrum of $\gamma$-$Al_2O_3$ is used as an approximation to $\Theta$-$Al_2O_3$.

contribute mainly to the CB DOS. Subtle differences in the total DOS of $\alpha$- and $\Theta$-$Al_2O_3$ can be seen. The O-2$s$ peak in $\Theta$-$Al_2O_3$ is lower than that in $\alpha$-$Al_2O_3$ by 1.0 eV. In the UVB region, $\Theta$-$Al_2O_3$ has a more broadened O-2$p$ nonbonding peak with a lower intensity. The three-peak structures in the lower portion of the CB DOS are similar in $\alpha$- and $\Theta$-$Al_2O_3$, though with different intensities. Another noticeable difference in the CB occurs at a higher energy. There is a sharp peak at 31 eV in $\alpha$-$Al_2O_3$. The same peak is shifted to 29 eV in $\Theta$-$Al_2O_3$ and is more broadened. As would be explained later, both are derived from Al-3$d$ orbitals.

The essential difference between $\alpha$- and $\Theta$-$Al_2O_3$ is that $\alpha$-$Al_2O_3$ has only $Al_{oct}$ atoms, while $\Theta$-$Al_2O_3$ has both $Al_{oct}$ and $Al_{tet}$ atoms. It is of interest to investigate the PDOS of Al at different sites. These are shown in Figs. 5(b) and 5(c). For comparison, the PDOS of octahedral Al in $\alpha$-$Al_2O_3$ is also shown in Fig. 5(a). Also shown as dotted lines are the sum of Al-$s$ and Al-$d$ components, which can be compared with experimental Al $L_{2,3}$ edge spectra to be discussed later. The PDOS of $Al_{oct}$ in both $\alpha$- and $\Theta$-$Al_2O_3$ are similar. Still, there are some subtle differences. Near the CB edge, a peak at 10 eV in $\alpha$-$Al_2O_3$ is absent in $\Theta$-$Al_2O_3$. This results in a less sharp absorption edge in $\Theta$-$Al_2O_3$. The Al-3$d$ peak at 29 eV in $\Theta$-$Al_2O_3$ is lower by 2 eV than in $\alpha$-$Al_2O_3$. This is consistent with the discussion on total DOS. The peak at 21 eV in $\Theta$-$Al_2O_3$, which is also contributed by Al-3$d$ orbitals is nonexistent in $\alpha$-$Al_2O_3$. Instead, there is a plateaulike region between 21 and 26 eV. On the other hand, the difference between the PDOS of $Al_{oct}$ and $Al_{tet}$ in $\Theta$-$Al_2O_3$ is much larger. The CB edge in the PDOS of $Al_{tet}$ is much more steep. There are extra sharp peaks located at 8.5, 16.5, and 25 eV. The peak at 29 eV in Fig. 5(b) is shifted upward to 30 eV and has a lower intensity. These features are indicated by arrows in Fig. 5. In the VB region, the PDOS of $Al_{oct}$ in both $\alpha$- and $\Theta$-$Al_2O_3$ have very similar features. The sums of Al-$s$ and Al-$d$ components contribute to the two peaks at $-2$ and $-7$ eV. This feature is not present in the PDOS of $Al_{tet}$.

Figure 6 shows the PDOS of $O_1$, $O_2$, and $O_3$ in $\Theta$-$Al_2O_3$. $O_1$ is fourfold coordinated and $O_2$, $O_3$ are threefold coordinated. For comparison, the PDOS of O in $\alpha$-$Al_2O_3$ is shown in Fig. 6(a). The dotted lines represent the O-$p$ component. The differences in the PDOS of different O atoms occur in the VB region. Figures 6(a) and 6(b) show the same O-2$p$ bonding and nonbonding characteristics since they correspond to the same O-$Al_4$ coordinations in $\alpha$- and $\Theta$-$Al_2O_3$.

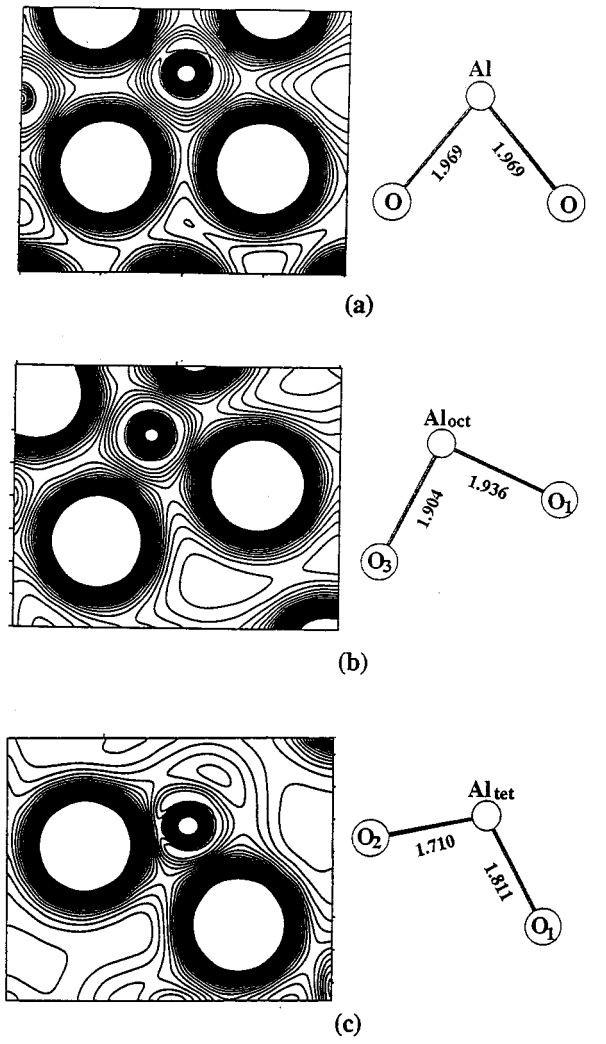


FIG. 9. Calculated valence charge density of $\alpha$- and $\Theta$-$Al_2O_3$ in three planes: (a) a plane containing two O and one Al in $\alpha$-$Al_2O_3$; (b) a plane containing $O_1$, $O_3$, and $Al_{oct}$ in $\Theta$-$Al_2O_3$, and (c) a plane containing $O_1$, $O_2$, and $Al_{tet}$ in $\Theta$-$Al_2O_3$. Contour lines are from 0.01 to 0.16 in the interval of 0.005 electron/(a.u.)$^3$.

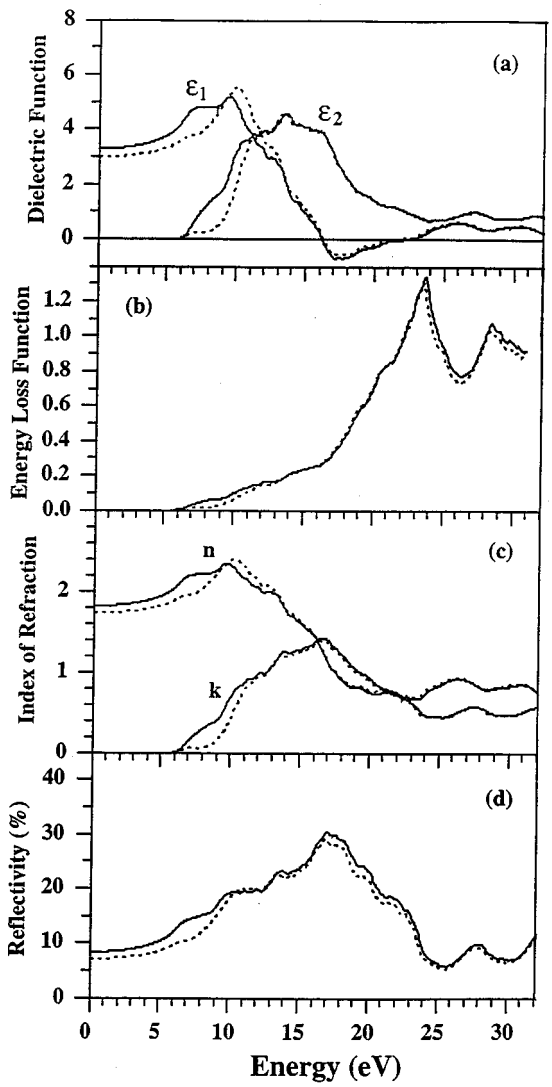


FIG. 10. Calculated optical properties of $\Theta$-$Al_2O_3$: (a) dielectric function; (b) energy loss function; (c) index of refraction; and (d) reflectivity. Solid (dotted) lines stand for the perpendicular (parallel) component.

The $O_2$ and $O_3$ atoms with different coordination in $\Theta$-$Al_2O_3$ show very different bonding and nonbonding features. In Fig. 6(c), the O-2$p$ bonding peak is sharper and has a higher intensity than the nonbonding peak. However, the O-2$p$ nonbonding peak in Fig. 6(d) is very sharp and has a much higher intensity, and the O-2$p$ bonding peak is almost invisible. The difference can be attributed to that O-$Al_{oct}$ bond is longer than the O-$Al_{tet}$ bond, and $O_2$ has two O-$Al_{tet}$ bonds and $O_3$ has only one O-$Al_{tet}$ bond. It is clear that the PDOS of Al and O are very much dependent on the short range order, or the local coordinations in alumina polymorphs.

In recent years, the use of electron-energy loss spectroscopy (EELS) with transmission electron microscope for materials research has greatly expanded. In particular, energy loss near edge spectroscopy (ELNES) measures the energy loss due to a transition of a specific core electron to the CB of the solid.[31] The technique has been applied as a fingerprinting of specific bonding types, especially for internal interfaces and grain boundaries. Because the core level states are localized, the symmetry-projected PDOS at the site of the excited atom subject to the dipole selection rule, is a reasonable approximation to the observed ELNES spectra. We shall compare the published Al $L_{2,3}$ edge (transition originates from the Al-2$p$ core level) and the O-$K$ edge (transition originates from the O-1$s$ core level), with the calculated Al $(s+d)$ PDOS and the O $p$ PDOS in the CB region. Since no ELNES data for $\Theta$-$Al_2O_3$ is available, the data for $\gamma$-$Al_2O_3$ are used instead.[32]

We compare the calculated CB PDOS (sum of $s$ and $d$ components) of Al in $\alpha$-$Al_2O_3$ [Fig. 7(a)] and in $\Theta$-$Al_2O_3$ [Fig. 7(b)] with the measure Al $L_{2,3}$ spectra.[32] For easy comparison, the first major peak in the experimental curves have been aligned with that of the PDOS. For $\alpha$-$Al_2O_3$, the calculated PDOS shows two distinct peaks at 14 and 30 eV. The ELNES spectrum also has two major peaks in the similar locations. The discrepancy occurs at the energy region between these two main peaks. The ELNES spectrum shows almost no intensity, while the calculated PDOS has additional structures in this region. A possible explanation for this is the neglect of the matrix element effect in approximat-

TABLE III. Calculated effective charges, bond orders, and static dielectric constants of $\alpha$- and $\Theta$-$Al_2O_3$.

| | $\alpha$-$Al_2O_3$ | | $\Theta$-$Al_2O_3$ | |
|---|---|---|---|---|
| | $Al_{oct}$: 1.90 (+1.10) | | $Al_{oct}$: | 1.95 |
| | | | $Al_{let}$: | 1.77 |
| Effective charge[a] | | | Average: | 1.86(+1.14) |
| | O: 6.74 (−0.74) | | $O_1$: | 6.73 |
| | | | $O_2$: | 6.81 |
| | | | $O_3$: | 6.75 |
| | | | Average: | 6.76(−0.76) |
| Bond order[b] | | | | |
| | | | $t$: | 0.264(1.710) |
| | | | | 0.141(1.745) |
| | | | | 0.115(1.811) |
| | | | Average: | 0.191(1.744) |
| | $o$: 0.101 (1.857) | | $o$: | 0.093(1.897) |
| | 0.081 (1.969) | | | 0.222(1.904) |
| | Average: 0.091 (1.913) | | | 0.084(1.936) |
| | | | | 0.161(2.025) |
| | | | Average: | 0.157(1.948) |
| Static dielectric constant $\epsilon_1(0)$[c] | ⊥: 3.27 | | | 3.01 |
| | ∥: 2.98 | | | |

[a]The numbers in parentheses are the effective valence charges.

[b]The numbers in parentheses are corresponding Al-O bond lengths in Å. $t(o)$ corresponds to tetrahedral (octahedral) bond.

[c]⊥(∥) are the perpendicular (parallel) component of static dielectric constant.

ing the PDOS for the ELNES spectrum. The experimental curves also show a very sharp peak at the edge which could originate from a core-hole excitons[5] that was not included in the calculation. For $\Theta$-$Al_2O_3$ [Fig. 7(b)], the calculated PDOS of Al has major structures roughly at 12, 14, 21, and 29 eV. The Al $L_{2,3}$ of $\gamma$-$Al_2O_3$ shows three major peaks. While the overall agreement is reasonable, the calculated PDOS again shows more structures than the ELNES data, especially in the region between the major peaks.

The ELNES of the O $K$ edges of $\alpha$- and $\Theta$-$Al_2O_3$ are shown in Fig. 8 together with the calculated O-$p$ PDOS in the CB. The main peak of O $K$ edge of $\alpha$-$Al_2O_3$ is broader and has a slightly different shape than that of $\Theta$-$Al_2O_3$. Our calculated PDOS's do reproduce this feature. Beyond the first major peak, the agreement between the general shape of calculated PDOS of O and ELNES O $K$ edge spectra is also quite reasonable.

### C. Effective valence charge and bond order

The nature of bonding in $Al_2O_3$ is an important issue and can be investigated quantitatively or semiquantitatively. In the OLCAO method, the Mulliken population analysis scheme provides the effective valence charge on each orbital $\rho_{\alpha i}$ of the atom $\alpha$, and on each atom $Q^*_\alpha$ as

$$\rho_{\alpha i}=\sum_{n,occ}\sum_{j,\beta} C^n_{i\alpha}C^n_{j\beta}S_{i\alpha,j\beta}, \tag{3}$$

$$Q^*_\alpha=\sum_i \rho_{\alpha i}, \tag{4}$$

where $C^n_{i\alpha}$ are the eigenvector coefficients for the state $n$ with atomic and orbital specifications of $\alpha$ and $i$, and $S_{i\alpha,j\beta}$ is the overlap matrix of the Bloch function. The bond order which qualitatively describes the strength of the bond between a pair of atoms can be defined as

$$q_{\alpha\beta}=\sum_{n,\mathrm{occ}}\sum_{i,j} C^n_{i\alpha}C^n_{j\beta}S_{i\alpha,j\beta}. \tag{5}$$

We have carried out separate minimal basis calculations for the effective charges and bond order in both crystals. It is well known that the Mulliken scheme is more valid when the basis functions are localized. Table III lists the calculated effective charges (or equivalently, the effective valence) and bond orders of $\alpha$- and $\Theta$-$Al_2O_3$. The average effective charges for both Al and O in the two crystals are quite close. However, $Al_{oct}$ in $\Theta$-$Al_2O_3$ has more charge than Al in $\alpha$-$Al_2O_3$, and $Al_{tet}$ has less charge than $Al_{oct}$ in $\Theta$-$Al_2O_3$. The $O_1$ atom in $\Theta$-$Al_2O_3$ has a similar effective charge as the O atom in $\alpha$-$Al_2O_3$, because of a similar fourfold coordination. The threefold coordinated $O_2$ and $O_3$ have larger effective charge than $O_1$. In sum, there is a larger charge transfer to O from Al in tetrahedral coordination than for an Al in octahedral coordination. For the crystal as a whole, the ionicity of $\Theta$-$Al_2O_3$ is comparable to that of $\alpha$-$Al_2O_3$. As far as bond order is concerned, the average bond order in $\Theta$-$Al_2O_3$ is larger than those in $\alpha$-$Al_2O_3$, because of the much shorter Al-O bonds in the $\Theta$ phase. In general, bond order increases when the coordination decreases, and bond length decreases. However, there can be exceptions. One of

the Al-O bonds of $Al_{oct}$ in Θ-$Al_2O_3$ is uncharacteristically large due to a more distorted nature of the octahedral coordination.

Figure 9 shows the calculated valence charge density of α- and Θ-$Al_2O_3$ in three planes: (a) a plane containing two O and Al in α-$Al_2O_3$; (b) the plane containing $O_1$, $O_3$, and $Al_{oct}$, and (c) a plane containing $O_1$, $O_2$, and $Al_{tet}$ in Θ-$Al_2O_3$. The difference in the charge distribution between α- and Θ-$Al_2O_3$ with Al in octahedral coordination is hardly visible. On the other hand, the valence charge distribution around the Al in the tetrahedral coordination [Fig. 9(c)] is noticeably different from that in octahedral coordination [Fig. 9(b)], and is consistent with a higher charge transfer at the tetrahedral site. Highly ionic features are evident for both crystals.

### D. Optical properties

The anisotropic optical properties in α-$Al_2O_3$ are very important because α-$Al_2O_3$ single crystal is optically uniaxial. Experimentally, Tomiki *et al.*[9] and French *et al.*[10] presented detailed investigations on this topic. In the earlier work of Ching and Xu,[11] the calculated optical properties of α-$Al_2O_3$ have been presented.[33] The emphasis of the present work is to focus on the anisotropy, and to compare with that of Θ-$Al_2O_3$ for which there is no experimental data. Figure 10 shows our calculated dielectric function, energy loss function, index of refraction, and reflectivity of α-$Al_2O_3$ up to a photon energy of 32 eV. The anisotropic features of these functions are demonstrated by the difference between the perpendicular (in solid lines) and parallel (in dotted lines) components. The perpendicular (parallel) component corresponds to the quantities measured for the electric field of light normal (parallel) to the $c$ axis of α-$Al_2O_3$. It is shown that the main differences between the parallel and perpendicular components occur at the photon energy region of less than 12 eV. They are almost identical in the region greater than 20 eV. The most prominent difference in the calculation is that the parallel component of $\varepsilon_2$ has a much sharper absorption edge than the perpendicular component. The electronic part of the static dielectric constant, taken as the zero frequency value of $\varepsilon_1$, is about 0.3 smaller for the parallel component than the perpendicular component. To compare the calculated anisotropy with the experimental data,[9] we focus on $\varepsilon_2$. The experimental data of Tomiki *et al.* show a much larger anisotropy, not only in the region close to absorption edge but also in the 10–20 eV region. The parallel component has two major peaks located at 13.11 and 16.94 eV and the perpendicular component have three peaks at 13.32, 14.91, and 17.35 eV. These fine features are not reproduced by our calculation, although our calculated $\varepsilon_2$ does reproduce the difference in the region closer to the absorption edge. It is possible that this less than satisfactory agreement is related to the inaccuracy of the wave functions obtained from the LDA calculation at high energies in the CB. On the other hand, French and co-workers[10] used two independent methods, VUV and EELS, to determine the optical properties of α-$Al_2O_3$. The measured reflectivity is close to the data of Tomiki *et al.* (Ref. 9). Our calculated optical spectra are in reasonable agreement with the experimental data of French *et al.*

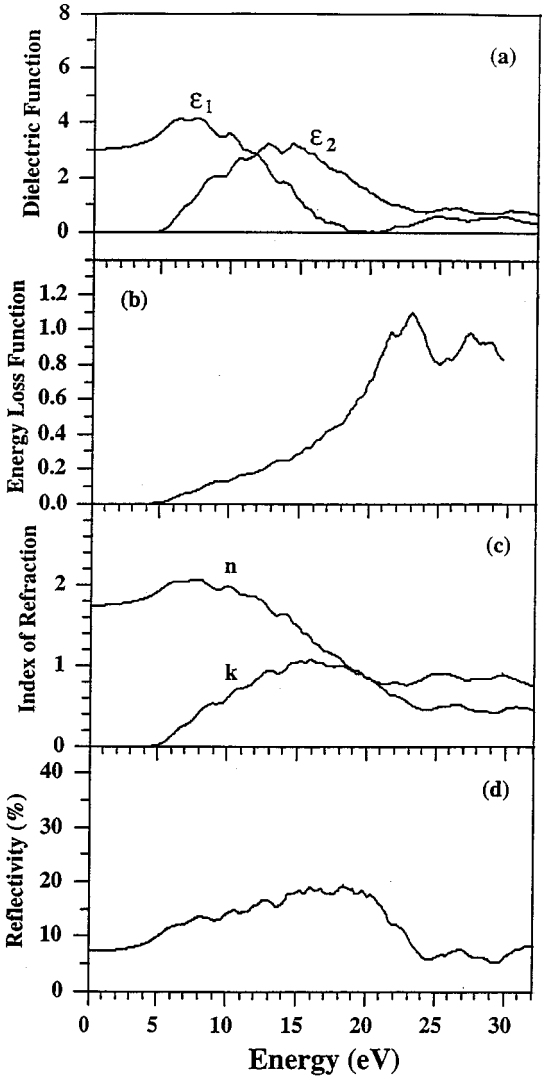


FIG. 11. Calculated optical properties of Θ-$Al_2O_3$: (a) dielectric function; (b) energy loss function; (c) index of refraction; and (d) reflectivity.

Figure 11 shows the calculated optical properties of Θ-$Al_2O_3$. The general features of the optical properties of α- and Θ-$Al_2O_3$ appear to be similar. Subtle differences in the structure can be identified. The $\varepsilon_2$ curve of Θ-$Al_2O_3$ is more broad and has a smaller amplitude than that of α-$Al_2O_3$. This is due to the band gap difference of about 1.6 eV and other differences in the electronic structure due to the presence of the tetrahedral sites in Θ-$Al_2O_3$. The plasmon peak in the energy loss function of Θ-$Al_2O_3$ is located at 22.6 eV, which is at a lower energy than the 23.5 eV in α-$Al_2O_3$. The calculated $x$, $y$, and $z$ components of the static dielectric constant of Θ-$Al_2O_3$ are found to be 3.01, 3.04, and 2.97, respectively. Therefore the anisotropic feature in the optical properties of Θ-$Al_2O_3$ is much less distinct than those in α-$Al_2O_3$. The averaged static dielectric constant of Θ-$Al_2O_3$ is 3.01, which is about 0.16 smaller than that of α-$Al_2O_3$. This means the estimated values of the ordinary refractive indices of 1.78 and 1.73 for α- and Θ-$Al_2O_3$, respectively. The lower refractive index for Θ-$Al_2O_3$ is consistent with its lower density. For the reflectivity, the value of Θ-$Al_2O_3$ is

about 10% larger than that of $\alpha$-$Al_2O_3$ within the photon energy region from 10 to 25 eV.

## IV. SOME CONCLUSIONS

We have presented a comparative study of the electronic and optical properties of $\alpha$- and $\Theta$-$Al_2O_3$ by means of first-principles calculations. Our results show that $\Theta$-$Al_2O_3$ has a smaller band gap than $\alpha$-$Al_2O_3$ but with comparable band structure parameters. The difference in the electronic properties is due to the different crystal structure and local short-range order in the two crystals. Total energy calculation predicts an energy difference of 1.47 eV per $Al_2O_3$ molecule between the $\Theta$ and $\alpha$ phases, accounting for the relative stability of the two phases at 0 K. Analysis of site- and orbital-resolved PDOS shows significant dependence of the PDOS for both Al and O atoms on their local coordinations, especially in the CB region. Effective charge calculation indicates $\Theta$-$Al_2O_3$ to be similar to $\alpha$-$Al_2O_3$. Our calculated orbital-resolved PDOS's are in reasonable agreement with experimental ELNES spectra of $\alpha$-$Al_2O_3$ and $\gamma$-$Al_2O_3$. An optical properties calculation on $\Theta$-$Al_2O_3$ shows it to be less anisotropic, and reflects the differences in the electronic structure with $\alpha$-$Al_2O_3$. The anisotropy in the optical properties of $\alpha$-$Al_2O_3$ occurs mainly at the low photon energy region of less than 12 eV.

The present study has been motivated by the desire to supply useful information about the $\gamma$-$Al_2O_3$ system. Being a structurally disordered system, the electronic and optical properties of $\gamma$-$Al_2O_3$ is much more difficult to calculate in the *ab initio* fashion. The present study is a step forward to a more comprehensive investigation on the structure and properties of $\gamma$-$Al_2O_3$, a system of considerable technological importance.

## ACKNOWLEDGMENT

This work was supported by the U.S. Department of Energy under Grant No. DE-FG02-84ER45170.

[1] W. H. Gitzen, *Alumina as a Ceramic Material* (American Ceramic Society, Columbus, OH, 1970), Special publication No. 4.
[2] E. Dörre and H. Hübner, *Alumina* (Springer-Verlag, Berlin, 1984).
[3] See, J. Am. Ceram. Soc. **77**, (2) (1994).
[4] K. Wefer and C. Misra, Alcoa Technical Paper No. 19, Alcoa Laboratories, 1972.
[5] I. Tanaka and H. Adachi, Phys. Rev. B **54**, 4604 (1996).
[6] J. C. Boettger, Phys. Rev. B **55**, 750 (1997).
[7] K. T. Thomson, R. M. Wentzcovitch, and M. S. T. Bukowinski, Science **274**, 1880 (1996).
[8] Y. Yourdshahyan, U. Engberg, L. Bengtsson, B. I. Lundquist, and B. Hammer, Phys. Rev. B **55**, 8721 (1997).
[9] T. Tomiki, Y. Ganaha, T. Shikenbaru, T. Futemma, M. Yuri, Y. Aiura, S. Sato, H. Fukutain, H. Kato, T. Miyahara, A. Yonesu, and J. Tamashiro, J. Phys. Soc. Jpn. **62**, 573 (1993); **62**, 1372 (1993).
[10] R. H. French, H. Müllejans, and D. J. Jones, J. Am. Ceram. Soc. (to be published).
[11] W. Y. Ching and Y.-N. Xu, J. Am. Ceram. Soc. **77**, 404 (1994).
[12] F. Robinson and M. Gillet, Thin Solid Films **98**, 179 (1982).
[13] Shang-Di Mo, Yong-Nian Xu, and Wai-Yim Ching, J. Am. Ceram. Soc. **80**, 1193 (1997).
[14] S. J. Wilson and J. D. C. McConnell, J. Solid State Chem. **34**, 315 (1980).
[15] R.-S. Zhou and R. L. Snyder, Acta Crystallogr., Sect. B: Struct. Sci. **47**, 617 (1991).
[16] E. Husson and Y. Repelin, Eur. J. Solid State Inorg. Chem. **33**, 1223 (1996).
[17] A. P. Borosy, B. Silvi, M. Allavena, and P. Nortier, J. Phys. Chem. **98**, 13 189 (1994).
[18] M. Wilson, M. Exner, Y.-M. Huang, and M. W. Finnis, Phys. Rev. B **54**, 15 683 (1996).
[19] R. W. G. Wyckoff, *Crystal Structures*, 2nd ed. (Wiley, New York, 1964), p. 274.
[20] F. S. Galasso, *Structure and Properties of Inorganic Solids* (Pergamon, New York, 1970).
[21] W. Y. Ching, J. Am. Ceram. Soc. **73**, 3135 (1990).
[22] Y.-N. Xu and W. Y. Ching, Phys. Rev. B **43**, 4461 (1991); **44**, 7787 (1991); **44**, 11 048 (1991); **48**, 4335 (1993); **51**, 17 379 (1995); H. Yao and W. Y. Ching, *ibid.* **50**, 11 231 (1994).
[23] W. Y. Ching and Y.-N. Xu, Phys. Rev. B **44**, 5332 (1991); Y.-N. Xu, W. Y. Ching, and R. H. French, *ibid.* **48**, 17 695 (1993); W. Y. Ching, Z.-Q. Gu, and Y.-N. Xu, *ibid.* **50**, 1992 (1994).
[24] S. Loughin, R. H. French, W. Y. Ching, Y.-N. Xu, and G. A. Slack, Appl. Phys. Lett. **71**, 2840 (1993); R. H. French, S. J. Glass, F. S. Oguchi, Y.-N. Xu, and W. Y. Ching, Phys. Rev. B **49**, 5133 (1994); W. Y. Ching, Y.-N. Xu, and R. H. French, *ibid.* **54**, 13 546 (1996).
[25] D. Li, Y.-N. Xu, and W. Y. Ching, Phys. Rev. B **45**, 5895 (1992); D. Li and W. Y. Ching, *ibid.* **52**, 17 073 (1995); **54**, 1451 (1996); **54**, 13 616 (1996).
[26] S.-D. Mo and W. Y. Ching, Phys. Rev. B **51**, 13 023 (1995); S.-D. Mo, W. Y. Ching, and R. H. French, J. Phys. D **29**, 1761 (1996).
[27] W. Y. Ching, Y.-N. Xu, and Z.-Q. Gu, Phys. Rev. B **54**, R15 585 (1996); Y.-N. Xu, Z.-Q. Gu, and W. Y. Ching, *ibid.* **56**, 14 993 (1997).
[28] G. Lehmann and M. Taut, Phys. Solid State **54**, 469 (1972).
[29] R. S. Mulliken, J. Am. Ceram. Soc. **23**, 1833 (1955); **23**, 1841 (1955).
[30] R. H. French, J. Am. Ceram. Soc. **73**, 477 (1990).
[31] R. F. Egerton, *Electron Energy Loss Spectroscopy in the Electron Microscopy*, 2nd ed. (Plenum, New York, 1996).
[32] I. Levin, W. D. Kaplan, D. G. Brandon, H. Müllejans, and M. Rühle, Mater. Sci. Forum **207-209**, 749 (1996).
[33] Due to a program error in the Kramas-Kronig transformation, the $\varepsilon_1$ calculated in Ref. 11 is not correct. The $\varepsilon_2$ is correct and is almost the same as in the present calculation.